Growth, crystal structure, and properties of the Li3Ba2Ln3(MoO4)8 (Ln = Er, Tm) molybdates

Pascale Armand, D. Granier, C. Reibel, M. Tillard

Growth, crystal structure, and properties of the $Li_3Ba_2Ln_3(MoO_4)_8$ (*Ln* = Er, Tm) molybdates

P. Armand*, D. Granier, C. Reibel, M. Tillard

ICGM, Univ. Montpellier, CNRS, ENSCM, Montpellier, France

ORCID: P. Armand 0000-0001-8921-5427,

M. Tillard 0000-0002-0609-7224

*Corresponding author: pascale.armand@umontpellier.fr

Abstract

The compounds $Li_3Ba_2Ln_3(MoO_4)_8$ (*Ln* = Er, Tm) have been obtained by the high-temperature flux technique using the slow cooling method. Crystals grown spontaneously were used to characterize the materials and investigate their properties using X-ray diffraction (XRD), Raman spectroscopy, and magnetic measurements. Single crystal structures were solved and refined in the monoclinic space group *C*2/*c*. Lattice dimensions are *a* = 5.1935, *b* = 12.6364, *c* = 19.1022 Å, β = 91.399 ° for Er-based triple molybdate (pink crystals) and *a* = 5.1846, *b* = 12.5766, *c* = 19.1557 Å, β = 91.525 ° for Tm-molybdate (green crystals). The *Ln* cations, mainly at general position 8*f*, are coordinated by eight oxygen atoms and adopt a distorted antiprismatic geometry. The distribution of atoms over the three cationic sites is discussed comparatively to literature reports. Unpolarized Raman characterization supports both the disordered cation distribution, and the distortion of the MoO_4 units. From the magnetic susceptibility measurements, it is found that the two triple molybdates follow a Curie-Weiss law in the 10 – 300 K domain, with a negative paramagnetic temperature θ_{CW}. The antiferromagnetic character is highlighted by the field-dependent magnetization curves.

Keywords

X-ray crystal structure; Raman investigation; Magnetic property

1. Introduction

The oxides containing lanthanide (*Ln*) ions are extensively investigated since they often show anomalous magnetic properties at low temperatures derived from the unpaired 4*f* electrons [1-4]. As there are seven 4*f* orbitals, the number of unpaired electrons can be as high as 7, which gives rise to the large magnetic moments observed for lanthanide compounds. Also, the photoluminescence properties of lanthanides are the subject of numerous studies with the growth of new crystallized phases. Some promising hosts for lanthanide luminescence are molybdates and tungstates as they have potentially favorable thermal and phonon properties depending on their structure type [5-7]. Furthermore, the interest in the double tungstate and double molybdate solids including a trivalent lanthanide (Ln^{3+}) has grown in importance as they are attracting materials for industrial applications with potential multifunctional physical properties depending on both the rare-earth element and the crystal structure [8-10]. The lithium rare-earth element double molybdates have also shown some interest as electrochemical anode materials in lithium-ion batteries [11].

On the other hand, very few studies are reported in the literature concerning the triple molybdates of general formula $A'_3A_2Ln_3(MoO_4)_8$ (where A' is a monovalent ion, A is a divalent ion, and *Ln* is a lanthanide element with the +3 oxidation number), and more precisely those with the composition $Li_3Ba_2Ln_3(MoO_4)_8$ [12-14]. These systems are likely to contain compounds with interesting physical properties and therefore deserve special attention.

The task of this work was to grow the new Li-based barium molybdate containing Er as the lanthanide element to study its structure and physical properties. We decided to prepare also crystals at the composition $Li_3Ba_2Tm_3(MoO_4)_8$ of which, to our knowledge, only the structure has been described [12]. The comparative study of the two compounds in terms of structure and physical properties could be used to assess effects due to the type of lanthanide. The technique

of crystal growth from a high temperature solution in an inorganic solvent (flux) with slow cooling has been used to produce single crystals of the triple molybdate [15].

This paper reports on the flux-growth synthesis and the crystal structure of the novel compound $Li_3Ba_2Er_3(MoO_4)_8$ and its Tm ternary molybdate analog. Their physical properties investigated by Raman spectroscopy and magnetic measurements are discussed based on literature reports

2. Experimental

2.1 Crystals preparation

The unseeded crystals have been spontaneously grown by the high-temperature self-flux technique using the slow cooling method. All the starting products are high purity level commercial powders (≥ 99%) and were used as received: $BaCO_3$ (Aldrich), Li_2CO_3 (Alfa Aesar), Er_2O_3 (Neyco), Tm_2O_3 (Neyco), and MoO_3 (Alfa Aesar). A mixture Li_2O-$3MoO_3$ was used as the self-flux and $Ba_3Ln_4O_9$ with *Ln* = Er, Tm as the solute, as we already synthesized these phases for previous works.

10 g of polycrystalline samples $Ba_3Ln_4O_9$ were prepared by a solid-state reaction from $BaCO_3$ and Ln_2O_3 thoroughly mixed in an agate mortar. An excess of $BaCO_3$ was added to compensate for the evaporation of barium. The mixture was inserted into a platinum crucible and placed in an electric furnace for thermal treatment: a 24 h-threshold at 850 °C followed by a 12 h-threshold at 1400 °C and then, a cooling rate of 300 °/h up to 20 °C was applied. The resulting product was checked by powder X-ray diffraction.

The flux was prepared by heating at 520 °C for 10 days a 1:3 mixture of Li_2CO_3 and MoO_3 in an electric furnace. The total mass of the flux prepared at a time was 100 g.

The spontaneous growth of the $Li_3Ba_2Ln_3(MoO_4)_8$ crystals was obtained from a 15 g mixture of the solute $Ba_3Ln_4O_9$ and the flux taken in a 10/90 weight ratio. The Pt crucible containing

this mixture was heated in air at 970 °C for 12h for homogenization, then slowly cooled down to 600 °C with a rate of 8 °/h. After, a cooling rate of 300 °/h was applied to reach the room temperature. The numerous and sub-millimeter-sized crystals grown at the surface of the solidified mixture (approximate yield of 30 %) were separated by dissolving the flux in water and then cleaned using a microwave bath.

We did not try to grow the bulk compounds by preparing in one step a mixture of the starting oxides Li_2O-BaO-Ln_2O_3-MoO_3 and then melting it before slow cooling, neither with a starting mixture consisting of $BaCO_3$ + Ln_2O_3 with the flux Li_2O-$3MoO_3$.

2.2 X-ray diffraction experiments

The crystalline and slightly colored platelets, either pink for the Er-compound or green for the Tm-compound were examined using a stereo microscope with a polarizing filter to select single crystals suitable for X-ray data collection. The diffracted intensities were measured at room temperature on an Xcalibur CCD (Oxford diffraction, MoKα radiation) diffractometer for the Er molybdate and on a D8 Venture equipment (Bruker, Incoatec micro source IμS 3.0, 110μm beam, Mo Kα, a Photon II CPAD detector) for the Tm compound. The data were processed with the appropriate software suite either using the CrysAlis or Apex software [16,17] for cell refinement, correction for Lorentz-polarization effects, and data reduction. An absorption correction was then applied using the included numerical (CrysAlis) or multi-scan (Bruker) procedures. According to the observed extinction conditions, the reflections were indexed in *C*2/*c* monoclinic cells with a = 5.1935(1), b = 12.6364(3), c = 19.1022(4) Å, β =91.399(1) ° for the Er compound, and a = 5.1846(1), b = 12.5766(2), c = 19.1557(3) Å, β = 91.525(4) ° for the Tm compound.

2.3 Raman measurements

The non-polarized Raman spectra were registered at room temperature in 180 ° back-scattering geometry with the help of a Horiba Jobin-Yvon LabRam Aramis confocal spectrometer equipped with an Olympus optical microscope and a Peltier-cooled charge-coupled device (CCD). For the two samples under study, Raman spectra were recorded using once the 473 nm excitation line of a blue diode laser, and once the 633 nm laser excitation source. The spectral resolution accuracy is of the order of ± 2 cm^{-1}. The Raman spectra were recorded for wavenumbers ranging from 50 to 4000 cm^{-1}.

2.4 Magnetic measurements

The dc-SQUID magnetometer Quantum Design MPMS 7XL was used for measurement of both the magnetization in the temperature range 1.8 - 300 K under an applied magnetic field of 500 Oe, and the field variation of the isothermal magnetization. Several crystals with a sub-millimeter size were weighted and blocked in a gelatin capsule and then inserted in a plastic straw. The total mass of crystals was 97.2 mg for $Li_3Ba_2Er_3(MoO_4)_8$ and 108.8 mg for $Li_3Ba_2Tm_3(MoO_4)_8$. No variation was observed between the data collected after cooling the sample in a magnetic field (FC) and the data collected after cooling in a zero field (ZFC).

3. Results and discussion

3.1 Crystal growth in flux

Visually transparent as-grown crystals were obtained *via* spontaneous nucleation from the high-temperature flux method. Most of the lanthanide ions exhibit characteristic colors when introduced into transparent solids. Crystals of the triple molybdate containing Er^{3+} ions are

pink/rose-colored with a millimeter size. Instead, the very pale green color of the flux-grown crystals is characteristic of Tm cations with the +3 oxidation state in $Li_3Ba_2Tm_3(MoO_4)_8$. The Tm-based oxides have a sub-millimeter size with a platelet form.

3.2 Crystal structure solution

The SHELX programs [18,19] were used to solve the structures and refine structural models by full-matrix least-squares methods. All the measured reflections were merged into a set of unique data used for refinements on F^2 that consider anisotropic displacement parameters for all atoms. The main parameters on diffraction measurements and crystal structure solution are given in Table 1.

Table 1 Crystal data and structure parameters for the $Li_3Ba_2Ln_3(MoO_4)_8$ molybdates

	$Li_{2.60}Ba_{2.17}Er_{3.02}(MoO_4)_8$	$Li_{1.98}Ba_{2.09}Tm_{3.28}(MoO_4)_8$
CSD number	2096264	2096265
Z	2	2
System, space group	monoclinic, *C*2/*c* (15)	monoclinic, *C*2/*c* (15)
***a* (Å)**	5.1935 (1)	5.1846 (1)
***b* (Å)**	12.6364 (3)	12.5766 (2)
***c* (Å)**	19.1022 (4)	19.1557 (3)
β (°)	91.400 (2)	91.525(4)
V (Å^3)	1253.24 (4)	1248.60 (4)
Crystal size (mm)	0.24 × 0.12 × 0.01	0.18 × 0.12 × 0.05
Diffractometer	Xcalibur Oxford diffraction	Bruker D8 VENTURE
Abs. correction ; μ (mm^{-1})	Numerical ; 17.31	Multi-scan ; 18.76
θ_{max}	32.45	40.31
Unique reflections	2119	3876
R_{int}	0.034	0.025
Refined param/restraints	118 / 5	118 / 5
R1, wR2 [I > 2σ(I)]	0.026, 0.068	0.019, 0.049
S	1.16	1.35
Δρ (e.Å^{-3})	1.38, −1.36	1.51, −1.19

For the Er– and Tm–lithium barium molybdates which are isostructural compounds, the structural model consists of 13 atomic positions of which two were readily attributed to molybdenum and 8 to oxygen atoms. The electron density peaks associated with the three remaining positions (M1, M2, and M3) were first ascribed respectively to Er (Tm), Ba, and Li atoms leading to R1 agreement factors of 5.8% (4.4%). Then a great improvement was observed when the corresponding site occupations were freed but the electric charge balance was not satisfied. At that time, complementary atomic mixing of Ln^{3+}, $Ba^{2+,}$ and Li^{+} cations was considered at the M1 and M2 positions. On the contrary, filling the M3 position with the heaviest cations would give rise to too short interatomic distances with the surrounding atoms, so that only lithium is considered at this site. The final refinements of the structural solution were carried using SUMP instructions to constrain the electric charge balance. The refined atomic positions and the equivalent thermal parameters are given in Table 2.

Table 2 Atom coordinates ($\times 10^4$) and equivalent displacement parameters ($Å^2 \times 10^3$) for $Li_3Ba_2Er_3(MoO_4)_8$ (**bold**) and $Li_3Ba_2Tm_3(MoO_4)_8$ (*italics*).

Atom	site	x	y	z	U_{eq}
M1	8*f*	**5025(1)**	**3525(1)**	**4685(1)**	**8(1)**
		5026(1)	*3521(1)*	*4687(1)*	*7(1)*
M2	4*e*	**0**	**-299(1)**	**2500**	**13(1)**
		0	*-309(1)*	*2500*	*12(1)*
M3	4*e*	**0**	**6851(12)**	**2500**	**43(4)**
		0	*6847(9)*	*2500*	*20(2)*
Mo1	8*f*	**-106(1)**	**5596(1)**	**4083(1)**	**9(1)**
		-115(1)	*5592(1)*	*4088(1)*	*8(1)*
Mo2	8*f*	**5005(1)**	**7606(1)**	**3509(1)**	**9(1)**
		5012(1)	*7596(1)*	*3518(1)*	*8(1)*
O1	8*f*	**2545(5)**	**5175(2)**	**4640(1)**	**15(1)**
		2569(3)	*5172(1)*	*4647(1)*	*13(1)*
O2	8*f*	**7565(5)**	**8529(2)**	**3652(2)**	**14(1)**
		7601(2)	*8521(1)*	*3662(1)*	*12(1)*
O3	8*f*	**3322(5)**	**7396(2)**	**4320(1)**	**13(1)**
		3293(2)	*7390(1)*	*4328(1)*	*11(1)*
O4	8*f*	**6407(5)**	**6440(2)**	**3215(2)**	**15(1)**

		6385(3)	*6418(1)*	*3229(1)*	*15(1)*
O5	8*f*	**1248(5)**	**5852(2)**	**3276(1)**	**15(1)**
		1234(3)	*5839(1)*	*3285(1)*	*14(1)*
O6	8*f*	**7666(5)**	**4546(2)**	**3951(2)**	**14(1)**
		7667(3)	*4535(1)*	*3961(1)*	*13(1)*
O7	8*f*	**8400(5)**	**6691(2)**	**4539(1)**	**14(1)**
		8384(2)	*6697(1)*	*4547(1)*	*11(1)*
O8	8*f*	**2269(5)**	**3007(2)**	**2126(2)**	**17(1)**
		2224(3)	*3008(1)*	*2119(1)*	*17(1)*

Atomic composition (%)

M1 **75.42 Er + 4.60 Ba + 19.98(1) Li** and *72.23 Tm + 16.09 Ba + 11.68(1) Li*

M2 **0.96 Er + 97.77 Ba +1.27(1) Li** and *20.16 Tm + 71.59 Ba + 8.25(1) Li*

M3 **89.44(2) Li** and *66.99(2) Li*

For the erbium compound, the refinement converged to an R1 agreement factor of 2.61% and the formula $Li_{2.60}Ba_{2.17}Er_{3.02}(MoO_4)_8$, atomic parameters are given in Table 2. In the case of the thulium compound, the refinement to R1 factor of 1.86% leads to the final formula $Li_{1.98}Ba_{2.09}Tm_{3.28}(MoO_4)_8$. These refined formulas are in fairly good agreement with the analysis performed on single crystals that gave an Er/Ba ratio of 1.35 and a Tm/Ba ratio of 1.25. Also, they do not deviate much from the general formula $Li_2Ba_2Ln_3(MoO_4)_8$. The quality of the experimental diffraction measurements and mainly the precision of analyzes performed on raw (not polished) surfaces of crystals could explain these results. More improbable reasons, as a composition variability between the crystals or the presence of Tm^{2+} cations (which we did not take into account in the electrical neutrality equation), were dismissed.

Note that the compounds are called $Li_3Ba_2Ln_3(MoO_4)_8$ in the following and that the full CIF files, deposited at the Cambridge Crystallographic Data Center [20], are freely available and can be obtained by simply providing the corresponding CSD numbers indicated in Table 1.

3.3 Structural description

The lithium barium erbium molybdate $Li_3Ba_2Er_3(MoO_4)_8$ is isostructural with its thulium analog, $Li_3Ba_2Tm_3(MoO_4)_8$. In their *C*2/*c* monoclinic structures, the atoms are located at 13

crystallographic independent positions listed in Table 2. The Mo atoms are distributed over two independent sites at 8*f* general positions and are coordinated by 4 oxygen atoms placed at distances ranging from 1.73 to 1.83 Å (Table 3), leading to slightly distorted tetrahedral environments around both the Mo1 and Mo2 positions.

Table 3 Bond lengths [Å] in $Li_3Ba_2Er_3(MoO_4)_8$ (**bold**) and $Li_3Ba_2Tm_3(MoO_4)_8$ (*italics*)

				Mo2–	O4	**1.743(3)**	*1.741(1)*
Mo1–	O5	**1.740(3)**	*1.735(1)*		O8	**1.747(3)**	*1.740(2)*
	O6	**1.774(3)**	*1.770(1)*		O2	**1.785(3)**	*1.792(1)*
	O1	**1.801(3)**	*1.812(1)*		O3	**1.815(3)**	*1.828(1)*
	O7	**1.819(3)**	*1.830(1)*				
				M2–	2 × O8	**2.656(3)**	*2.651(1)*
M1–	O2	**2.325(3)**	*2.303(1)*		2 × O4	**2.679(3)**	*2.670(1)*
	O3	**2.349(3)**	*2.330(1)*		2 × O5	**2.873(3)**	*2.883(2)*
	O7	**2.359(3)**	*2.343(1)*		2 × O2	**2.961(3)**	*2.968(1)*
	O6	**2.367(3)**	*2.353(1)*		2 × O6	**3.074(3)**	*3.095(1)*
	O3	**2.372(3)**	*2.355(1)*				
	O1	**2.423(3)**	*2.410(1)*	**Li–**	2 × O5	**2.041(10)**	*2.055(7)*
	O1	**2.450(3)**	*2.436(1)*		2 × O8	**2.146(11)**	*2.163(7)*
	O7	**2.480(3)**	*2.458(1)*		2 × O4	**2.396(5)**	*2.428(3)*

These MoO_4 tetrahedra occur in the structure as discrete polyhedral units and their arrangement in the unit cell leaves room for cation hosting as shown in the DIAMOND [21] structural representation of the unit cell given in Figure 1. The cations Ln^{3+}, Ba^{2+}, and Li^{+} filling the voids between tetrahedral MoO_4 units are distributed over three independent positions, at one 8*f* and two 4*e* crystallographic sites.

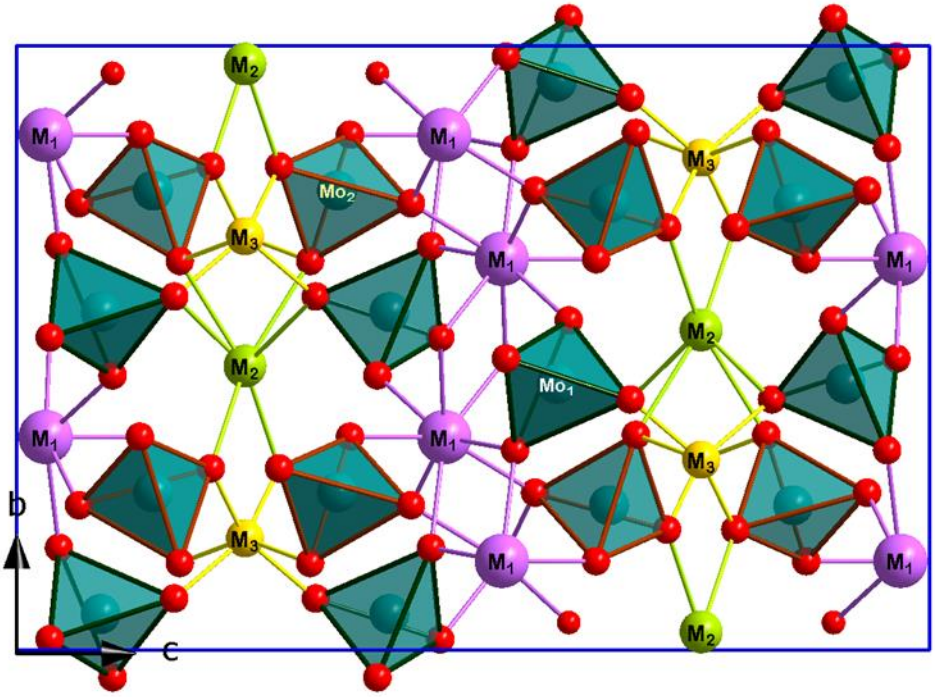

Figure 1 The arrangement of MoO_4 tetrahedra in the monoclinic structure of $Li_3Ba_2Ln_3(MoO_4)_8$. Cationic positions M1 (violet), M2 (green), and M3 (yellow) are drawn with their bonds to oxygen in a unit cell projection along the *a*-axis.

The M1 general 8*f* position mainly filled with *Ln* (~75%) is surrounded by eight oxygen atoms, placed at distances from 2.30 to 2.48 Å, which form a coordination polyhedron that can be viewed as a fairly distorted square antiprism (with no special symmetry) drawn in Figure 2.

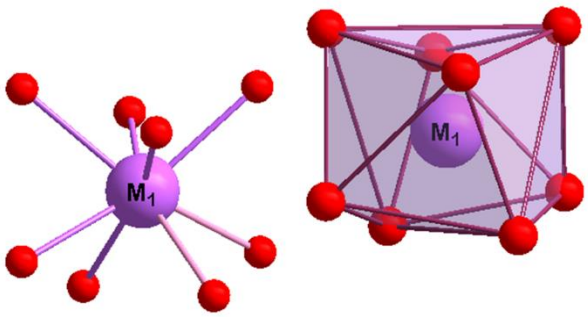

Figure 2 Oxygen environment and coordination polyhedron around the position M1

This LnO_8 unit shares oxygen atoms (one common edge) with each of the three adjacent units inside the Ln^{3+} cationic layer involving M1 atoms (Figure 3) leading to Ln^{3+}---Ln^{3+} interactions of 3.82, 3.89, and 3.91 Å for the Er-compound and 3.80, 3.88 and 3.91Å for the Tm-compound.

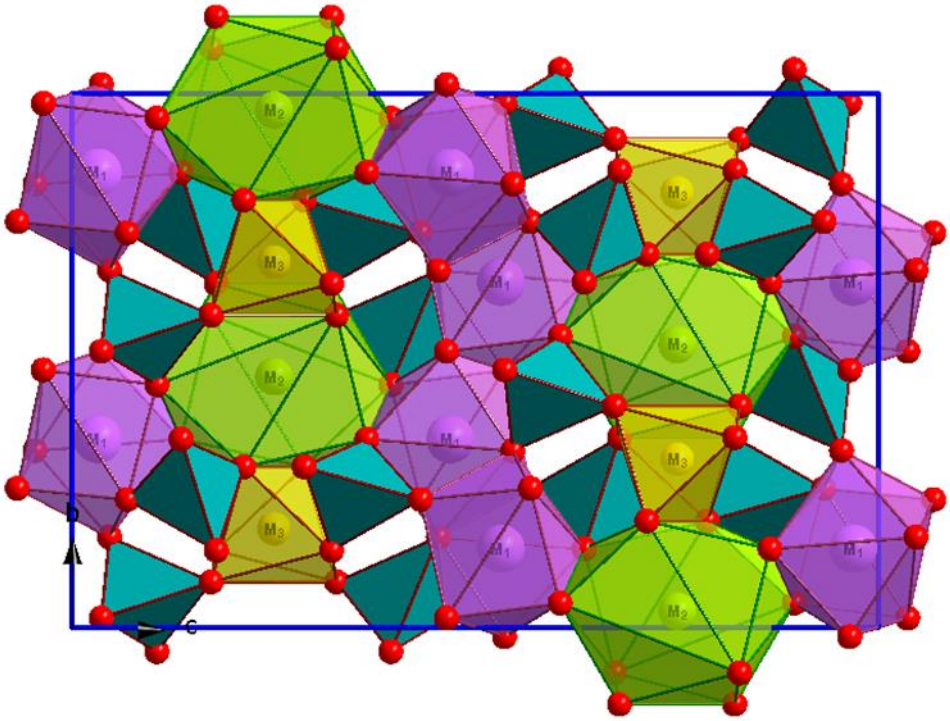

Figure 3 Coordination polyhedra around Mo (blue), M1 (*Ln*, violet), M2 (Ba, green), and Li (yellow) in $Li_3Ba_2Ln_3(MoO_4)_8$ with *Ln* = Er, Tm (projection in (011) plane).

The M2 site mainly filled with Ba is surrounded by ten oxygen atoms, at distances between 2.65 and 3.10 Å, arranged in a sort of pentagonal antiprism (Figure 4) with 2-fold symmetry as centered at the 4*e* site (0, x, ¼). It is represented as a green polyhedron in Figure 3.

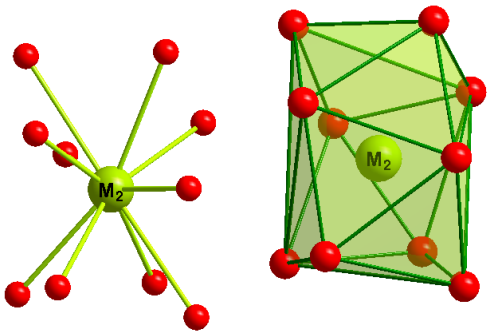

Figure 4 Oxygen environment and coordination polyhedron around the position M2

Interestingly, the M2 site is occupied with a proportion of about 20% of Tm^{3+} ions in the Li-Ba-Tm triple molybdate while, in the Er compound, only ~1% of Er^{3+} lanthanide cations is found at this site, Table 3. Thus it is important to note that two environments are to be taken into account for the Tm^{3+} ions occurring in the two nonequivalent geometries TmO_8 and TmO_{10}, shown in Figure 2 and Figure 4.

Finally, also located at a 4*e* special position, the M3 site offers voids that are only appropriate for Li cations surrounded by six oxygen atoms (2.04-2.43 Å) forming a distorted octahedron with 2-fold symmetry represented in Figure 5 and shown as a yellow polyhedron in Figure 2.

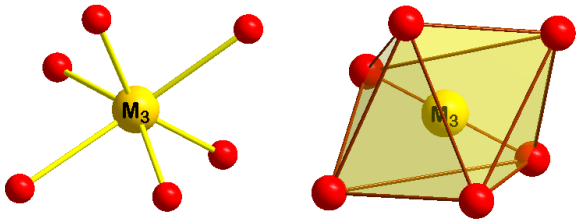

Figure 5 Oxygen environment and coordination polyhedron around Li atoms (M3 site)

At this stage, the structural results obtained in the current study from single-crystal diffraction data deserve to be compared with previous data from the literature. Looking at the atomic positions, our structural model is identical to that provided 20 years ago for single-crystals of the ternary molybdates $Li_3Ba_2Ln_3(MoO_4)_8$ with *Ln* = Gd and Tm [12]. In this earlier work, the distribution of the cations over the M sites was based on empirical considerations (local valence force balance), and the *Ln*:Ba:Li cationic proportions (67.5:7.5:25.0 at M1, 15:85:0 at M2, and 0:0:100 at M3) were kept fixed during the structural refinements setting thus the *Ln*/Ba ratio to 1.5. We tried to apply such fixed cationic contents but the structural refinements with our diffraction data led to an R1 factor of 3.6% with too high displacement parameters at M3 and the presence in the Fourier difference of residual positive and negative abnormal electronic densities located very close to M1 and M2 positions. This result is not acceptable and not as

good as when the atomic contents have been refined, converging to Er:Ba:Li ratios of 75.4:4.6:20.0 at M1, 0.9:97.8:1.3 at M2, and 0:0:89.4 at M3 with a final R1 of 2.61%.

Similar behavior (high-density peak close to M1, deep hole very close to M2 and R1 of 4.07%) was found for the Tm molybdate for which, in our refinement conditions, the cation proportions converged to 72.2:16.1:11.7 at M1, 20.2:71.6:8.2 at M2 and 0:0:70 at M3 and R1 to 1.88%.

A recent work reports the structural study of a Yb-doped $Li_3Ba_2Gd_3(MoO_4)_8$ crystal [14] with a mixture Yb:Gd:Li at site M1, pure Ba at site M2, and pure Li at site M3. Refining our data in this way was not fully satisfactory, due in particular to a remaining density at the M2 position. Besides, another work published in 2019 [22] states that the Li content is parted over the M1 and M3 sites in the proportion ⅓ ⅔, that *Ln* completes the site M1 and that Ba/Sr fill the site M2 in the isotype monoclinic structure of $Li_3BaSrGd_3(MoO_4)_8$.

Valence numbers of 5.7 and 5.8 have been calculated for Mo sites in the two compounds using the bond valence method [23]. Such valence sum analysis clearly depends on two parameters, (R_0 and b) empirically determined and we used their more recently tabulated values [24]. At the mixed Ln/Ba/Li site M1, the calculated valence numbers are close for the two compounds (2.6 and 2.8) while they differ slightly at site M2 (2.3 and 1.9) in good agreement with the lower Ba^{2+} content at this position in the Tm compound, according to the structural refinement.

In brief, the common points between all these experimental results relative to isostructural compounds are that *Ln* is the major component at site M1, Ba dominates at site M2 and only Li is found at site M3. It can be concluded at this point that the cation distribution in such ternary molybdates could be rather complex and may differ for the various compositions. Yet, both the final refined formulas of the ternary molybdates studied in the current work, $Li_{2.60}Ba_{2.17}Er_{3.02}(MoO_4)_8$ and $Li_{1.98}Ba_{2.09}Tm_{3.28}(MoO_4)_8$, and those described in the literature do not deviate much from the general stoichiometry $Li_3Ba_2Ln_3(MoO_4)_8$.

The structural packing made of tetrahedral MoO_4 units arranged in the unit cell leaves voids that can accommodate the different cations depending on their size. It is obvious that the voids around the M3 positions are not large enough to accept big cations as Ln^{3+} or Ba^{2+}, only the smallest Li^+ cations (ionic radius 0.76 Å in CN6 environment [25]) could fit. As shown by the various structural studies (current work and refs [12, 14, 22]), the large Ba^{2+} cations (1.52 Å in CN10) display a site preference for the M2 position they occupy either alone or in major proportion. Instead, the cavities around the M1 position suit better to the Ln^{3+} cations with medium sizes (0.985 Å for Yb^{3+}, 0.994 for Tm^{3+}, 1.004 for Er^{3+} and 1.053 for Gd^{3+} in CN8) which explains their presence in greater proportion at this position. Cationic vacancies were never considered at M1 and M2 sites as the total population are always assumed equal to unity (incomplete filling with atomic mixing would be hard or impossible to model in the structural refinements). Nevertheless, a progressive loss of Li is mentioned in the study of the gadolinium triple molybdate [14]. When prepared at relatively low temperatures and annealed for a long time, the final compound is $Li_3Ba_2Gd_3(MoO_4)_8$ while the samples obtained at higher temperatures are suspected to be Li-free and correspond to the double molybdate $Ba_2Gd_4(MoO_4)_8$ where the Gd^{3+} cations fill the M1 site, the Ba^{2+} cations fill the M2 site and in which the M3 site remains empty [26]. This may support the partial filling of the M3 site as found in our refinements for the Er and Tm molybdates but also gives strong arguments to consider various possibilities for the cationic distribution over the M sites. Such different distributions could result from the experimental conditions such as the heating temperature or the annealing treatments used for the synthesis of the compounds. These experimental observations for very similar compounds belonging to the $Li_3Ba_2Ln_3(MoO_4)_8$ ternary molybdates family are the mark of a certain degree of adaptability of the structure, able to accommodate various cationic contents at these positions, and therefore to deviate slightly from the general formula.

3.4 Raman spectroscopy

As the as-grown crystals are colored due to the presence of lanthanide ions, pink color for Er^{3+} and pale green for Tm^{3+}, we have collected the room temperature Raman spectra using two distinct excitation wavelengths, 473 and 633 nm, Figure 3.

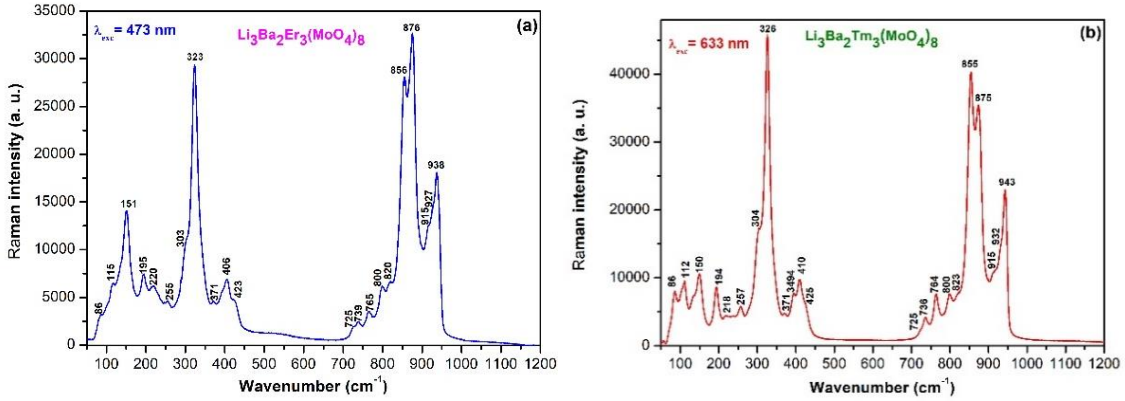

Figure 6 Unpolarized Raman spectrum registered at room temperature on an as-grown sub-millimeter crystal of (a) $Li_3Ba_2Er_3(MoO_4)_8$ and (b) $Li_3Ba_2Tm_3(MoO_4)_8$.

The two spectra, taken in air, show a very strong resemblance, with bands displaying a large full width at half maximum (FWHM). The frequency of the vibration modes is only slightly affected by the kind of the rare-earth ion. This is certainly because the lanthanides Er and Tm are placed side by side in the periodic table. The large bands support the disordered statistical distribution of the cations at sites 8*f* and 4*e* in the monoclinic structure. Moreover, the Mo atoms are distributed over two independent sites at 8*f* general positions of symmetry 1 (C_1).

The first group of bands lying in the high frequency domain, 720 – 950 cm^{-1}, are attributed to the internal symmetric and antisymmetric stretching vibrations of the Mo-O bonds in the tetrahedral MoO_4 entities based on literature data [27, 28], Figure 6. The complexity of the spectra is well explained by the degeneracy removal of the Mo-O stretching modes due to the symmetry lowering ($Td \rightarrow C_1$) of the MoO_4 tetrahedra (Mo in 8*f* general position). Actually, a free tetrahedral MoO_4^{2-} anion having the *Td* symmetry is characterized by a $\nu_1(A1)$ symmetric

stretching at 936 cm^{-1} and a $\nu_3(T2)$ antisymmetric stretching at 895 cm^{-1} while up to four lines can be present in the symmetric stretching domain and up to 12 in the asymmetric range for MoO_4 units with symmetry C_1 [29].

The lack of Raman bands in the middle frequency range 500 – 700 cm^{-1} for the two materials under study is consistent with the fact that the Mo^{6+} ions coordinated with oxygen result in isolated tetrahedral MoO_4^{2-} polyhedra. As Mo-O-Mo bridges are not present in these structures, the Raman fingerprints due to the asymmetric vibrations ν_{as}(Mo-O-Mo) expected near 620 cm^{-1} are absent from their spectra [30].

The bands in the range 200 – 450 cm^{-1} are assigned to the internal asymmetric and symmetric bending vibration δ(O-Mo-O) of the MoO_4 tetrahedra [28, 29]. Below 200 cm^{-1}, the bands are due to external vibrations that involve the rotational and translational modes of the MoO_4^{2-} anions and the translational modes of cations [28].

3.5 Magnetic properties

The dc-magnetization data were registered with an external magnetic field H = 500 Oe in a temperature range from 1.8 to 300 K. The dependence in temperature of both the zero-field-cooled magnetic susceptibility χ and the inverse of susceptibility χ^{-1} is presented in Figure 7 for $Li_3Ba_2Ln_3(MoO_4)_8$, *Ln* = Er, Tm. χ^{-1} follows a linear dependence with temperature in the 10 − 300 K paramagnetic region. A change in the regime is observed in the very low temperature range ($1.8 \leq T < 10$ K): χ^{-1} makes a down-turn for *Ln* = Er, Figure 7(a), and an up-turn for *Ln* = Tm, Figure 7(b).

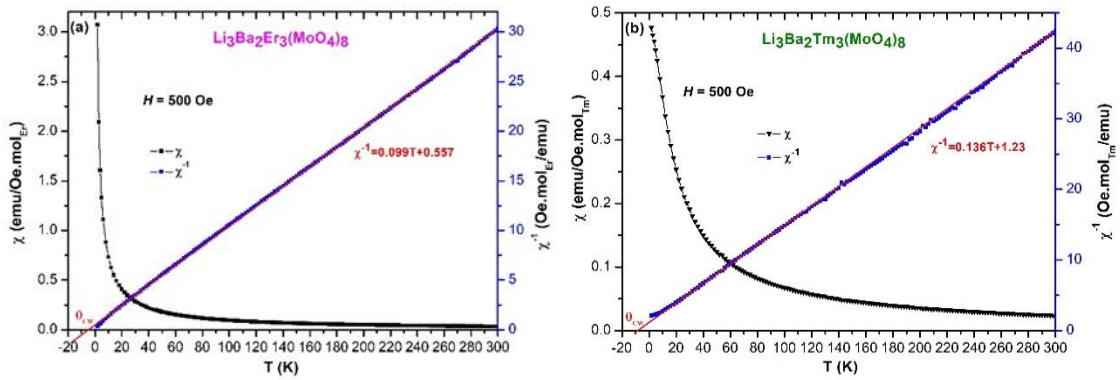

Figure 7 The dc susceptibility (χ) and its inverse (χ^{-1}) at constant field *vs*. temperature for $Li_3Ba_2Ln_3(MoO_4)_8$ showing a Curie-Weiss behavior (red line). *Ln* = Er (a); *Ln* = Tm (b)

For the two triple molybdates understudy, the paramagnetic region corresponding to the 10 - 300 K temperature range has been fitted with a Curie-Weiss law $\chi = C/(T - \theta_{CW})$ where C is the Curie constant and θ_{CW} the paramagnetic Curie temperature. The experimental effective magnetic moments, μ_{eff}, are calculated from the Curie constant according to the formula $\mu_{eff} = (8 \times C)^{1/2}$. The least-squares parameters used in the curve fitting are gathered in Table 4.

Table 4 Effective magnetic moments, and least-squares parameters from the inverse susceptibility χ^{-1} curves fitting.

	C (emu.K.mol^{-1})	**θ_{CW} (K)**	**μ_{eff} (μB/*Ln*-atom)**
$Li_3Ba_2Er_3(MoO_4)_8$	10.10	−5	8.99
$Li_3Ba_2Tm_3(MoO_4)_8$	7.25	−9	7.61

The experimental effective magnetic moments μ_{eff} at room temperature, Table 4, are comparable to their theoretical counterparts (within the limits of experimental errors), namely, 9.57 for the free cation Er^{3+} and 7.63 for the Tm^{3+} free-ion, which confirms the Ln^{3+} oxidation state. This indicates that in the paramagnetic state, only the Ln^{3+} ions contribute to the magnetic moment in the two $Li_3Ba_2Ln_3(MoO_4)_8$ structures under study as molybdenum, formally in the

+6 oxidation state, does not carry any magnetic moment. The magnetic moments arise from the ground electronic states of the electronic configuration $4f^n$ of the trivalent rare-earth ions, with $n = 11$ for Er and $n = 12$ for Tm.

The negative values of θ_{CW} obtained for the two lanthanide triple molybdates are very close, Table 4, and suggest that the two samples present, below 12 K, antiferromagnetic interactions between the Ln^{3+} magnetic moments. The decrease in the absolute value of θ_{CW} indicates a weakening of the antiferromagnetic interactions from *Ln* = Tm to *Ln* = Er.

The deviation from the Curie–Weiss law appears at 10 K and 12 K for *Ln* = Er and Tm, respectively. The start of the upward-turn of the inverse susceptibility curve for *Ln* = Tm at liquid hydrogen temperatures, Figure 7(b), could be associated with the transition temperature from paramagnetic to antiferromagnetic, called the Néel temperature T_N. Inversely, the down turn for *Ln* = Er, Figure 7(a), may be due to crystal field (CF) effects which can affect the ground state of the magnetic ion at low temperatures. Indeed, when a rare-earth ion is placed in a crystal lattice, it is subjected to a number of forces which are absent in the free ion.

The magnetization isotherms recorded at 300 K and at 50 K for $Li_3Ba_2Ln_3(MoO_4)_8$ (Ln = Er, Tm), Figure 8, are linear functions of the applied external magnetic field H in accordance with a paramagnetic behavior. With the increase in the magnetic field at liquid helium temperatures, the polarization of local magnetic moments of $Ln3^+$ ions induced by the external-field also increases. The hysteresis loops plotted for the Tm-based compound at $T < 50$ K are very similar, and do not show coercive field neither magnetic saturation even at the lowest temperatures, Figure 8(b). Concerning the Er-based molybdate, the M-H curves registered at $T \leq 10$ K display a large field dependence, Figure 8(a). For T = 1.8 and 2 K, in weak fields, the magnetization is proportional to the field. A change occurs in the slope of the magnetization curve around H =10 kOe, and the magnetization get saturated at 20 kOe. Such variation may indicate the existence of an antiferromagnetic component to the long range order.

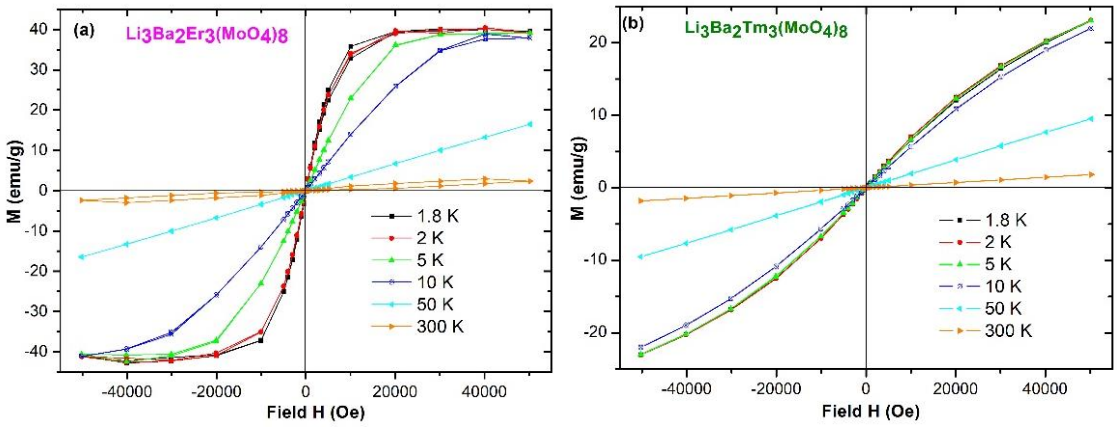

Figure 8 Isothermal magnetization *vs.* applied magnetic field (1.8 to 300 K) for $Li_3Ba_2Ln_3(MoO_4)_8$. *Ln* = Er (a); *Ln* = Tm (b)

The magnetic behavior of the two triple molybdates under study is determined by the magnetic properties of their lanthanide ion which, at liquid helium temperatures, may be sensitive to the crystal-field (CF) effect which affects the energy levels of the Ln^{3+} ion. The strength of the CF effect depends on the bonding geometry of the Ln^{3+} ions and the nature of its bonding interactions. The distribution of the Tm^{3+} cations in $Li_3Ba_2Ln_3(MoO_4)_8$ over two distinct positions (8*f* and 4*e*, Tm^{3+} site disorder) gives rise to two types of Tm occurring in the nonequivalent geometries TmO_8 and TmO_{10}, unlike the Er^{3+} cations found almost fully distributed over the 8*f* crystallographic site (no significant Er^{3+} site disorder). Therefore, the splitting scheme of the $^3H_6$ ground state of thulium by the crystal electric field should differ from that of the state $^4I_{15/2}$ of erbium. Then, the saturation of the magnetization observed for the Er compound at low temperatures and high field, Figure 8(a), could be attributed to a complete filling of the ground state energy levels. Instead, the splitting scheme of Tm^{3+} ion would prevent saturation for occurring at equivalent temperatures and external magnetic fields, Figure 8(b).

The disparity in magnetic behavior between these two compounds provides evidence that changing the nature of the Ln^{3+} ions and its environments has an impact on the physical properties of $Li_3Ba_2Ln_3(MoO_4)_8$ with *Ln* = Er, Tm. A more rigorous investigation of the magnetic interactions, and the magnetic unit cell, is needed to elucidate all interactions present.

4. CONCLUSION

High-quality single crystals with the general formula $Li_3Ba_2Ln_3(MoO_4)_8$ ($Ln = Er^{3+}$, Tm^{3+}) were obtained by spontaneous growth from a high-temperature method using a Li_2O-$3MoO_3$ flux. The $Li_3Ba_2Er_3(MoO_4)_8$ crystal structure was refined for the first time with data recorded in a single-crystal X-ray diffraction experiment. The compounds crystallize in the centrosymmetric space group $C2/c$ and the Ln^{3+}, $Ba^{2+,}$ and Li^+ cations are spread over three distinct cationic sites (two positions with statistical disorder and one with only Li^+). The Mo centers (Mo^{6+} ions) distributed over two independent sites form isolated MoO_4 tetrahedra with oxygen. Unpolarized Raman spectra agree with the isostructural atomic arrangement in the two phases and support both the disordered cationic distribution and the distortion of the MoO_4 units. The small paramagnetic Curie - Weiss temperatures θ_{CW} obtained suggest an antiferromagnetic coupling between the Ln^{3+} below ~12 K for the two compounds. Neutron-diffraction measurements for $Li_3Ba_2Ln_3(MoO_4)_8$ ($Ln = Er^{3+}$, Tm^{3+}) should be undertaken to establish the magnetic structures of these materials.

Acknowledgments

Raman and magnetic measurements were done at the Platform of Analysis and Characterization (PAC) of the Pôle Chimie Balard in Montpellier, France. The single-crystal X-ray diffraction experiments were done using the technological resources of the X-ray and gamma-ray network at the University of Montpellier, France.

Funding

This work was supported by the French Ministry of Higher Education, Scientific Research and Innovation, and the French National Center of Scientific Research (CNRS).

References

[1] Crystal structures and magnetic properties of magnetically frustrated systems $BaLn_2O_4$ and $Ba_3Ln_4O_9$ (Ln = lanthanide)
Yo s h i hiro Doi, Wataru Nakamori, Yukio Hinatsu
J. Phys.: Condens. Matter 18 (2005) 333
10.1088/0953-8984/18/1/024

[2] Antiferromagnetism of double molybdate $LiFe(MoO_4)_2$
M. Liu, Y. Zhang, T. Zou, V. Ovidiu Garlea, T. Charlton, Y. Wang, F. Liu, Y. Xie, X. Li, L. Yang, B. Li, X. Wang, S. Dong, J.-M. Liu
Inorg. Chem. 59 (2020) 8127 - 8133.
10.1021/acs.inorgchem.0c00432

[3] Crystal growth, crystal structure, and anisotropic magnetic properties of $KBaR(BO_3)_2$ (R = Y, Gd, Tb, Dy, Ho, Tm, Yb, and Lu) triangular lattice materials
S. Guo, T. Kong, F. Alex Cevallos, K. Stolze, R. J. Cava
J. Magn. Magn. Mater**.** 472 (2019) 104 -110
10.1016/j.jmmm.2018.10.037

[4] Cycloidal magnetism driven ferroelectricity in double tungstate $LiFe(WO_4)_2$
M. Liu, L. Lin, Y. Zhang, S. Li, Q. Huang, V. O. Garlea, T. Zou, Y. Xie, Y. Wang, C. Lu, L. Yang, Zhibo Yan, Xiuzhang Wang, Shuai Dong, J. Liu less
Phys. Rev. B (2017) 195134.
10.1103/PhysRevB.95.195134

[5] The optical spectroscopy of lanthanides R^{3+} in $ABi(XO_4)_2$ (A = Li, Na; X = Mo, W) and $LiYb(MoO_4)_2$ multifunctional single crystals: Relationship with the structural local disorder.
C. Cascales, A. Méndez Blas, M. Rico, V.Volkov, C. Zaldo
Opt. Mater. 27 (2005) 1672-1680.
10.1016/j.optmat.2004.11.051

[6] Triple molybdates and tungstates scheelite structures: Effect of cations on structure, band-gap and photoluminescence properties
Bal Govind Vats, Muhammed Shafeeq, Swayam Kesari
J. Alloys Compd 865 (2021) 158818
10.1016/j.jallcom.2021.158818

[7] Structure and luminescent properties of three new silver lanthanide molybdates.
F. Shi, J. Meng, Y. Ren
J. Solid State Chem. 121 (1996) 236-239.
10.1006/jssc.1996.0033

[8] Growth, structure, and evaluation of laser properties of $LiYb(MoO_4)_2$ single crystal.
V. Volkov, C. Cascales, A. Kling, C. Zaldo
Chem. Mater. 17 (2005) 291-300.
10.1021/cm049095k

[9] Double tungstate and molybdate crystals for laser and nonlinear optical applications
E.V. Zharikov, C. Zaldo, F. Diaz
MRS bulletin 34 (2009) 271-276.
10.1557/mrs2009.78

[10] AC impedance analysis of $LaLiMo_2O_8$ electroceramics
S. Brahma, R.N.P. Choudhary, A. K. Thakur
Physica B: Condensed Matter 355 (2005) 188-201.
10.1016/j.physb.2004.10.091

[11] $LiFe(MoO_4)_2$ as a novel anode material for Lithium-Ion Batteries.
N. Chen, Y. Yao, D. Wang, Y. Wei, X. Bie, C. Wang, G. Chen, F. Du
ACS Appl. Mater. Interfaces 6 (2014) 10661-10666.
10.1021/am502352c

[12] Crystal structure investigation of ternary molybdates $Li_3Ba_2Ln_3(MoO_4)_3$ (Ln=Gd, Tm)
R. F. Klevtsova, A. D. Vasil'ev, L. A. Glinskaya, A. I. Kruglik, N. M. Kozhevnikova, V. P. Korsun
J. Struct. Chem. 33 (1992) 443–447.
10.1007/BF00748057

[13] Growth and spectral properties of Nd^{3+}-doped $Li_3Ba_2Ln_3(MoO_4)$ (Ln = La, Gd) crystals
Mingjun Song, Lizhen Zhang, Guofu Wang
J. Alloys Compd 480 (2009) 839-842.
10.1016/j.jallcom.2009.02.082

[14] Crystal Growth and Optical and Spectroscopic Characterization of the Ytterbium-Doped Laser Molybdate $Yb{-}Li_3Gd_3Ba_2(MoO_4)_8$
A. García-Cortés, C. Cascales
Chem. Mater. 20 (2008) 3884 – 3891.
10.1021/cm703138x

[15] Obtention de monocristaux au sein d 'un flux fondu
Y. Laurent
Rev. Chim. Miner. 6(6) (1969) 1145-1186

[16] CrysAlis'Red' 171 software package,
Oxford Diffraction Ltd, Abingdon, United Kingdom, (2004).

[17] Bruker, APEX3. Version 2017.3-0, Bruker AXS, Inc., Madison, Wisconsin, USA, 2017

[18] Crystal structure refinement with SHELXL
G. M. Sheldrick
Acta Crystallogr. C71 (2015) 3-8
10.1107/S2053229614024218

[19] SHELXT - Integrated space-group and crystal-structure determination
G. M. Sheldrick
Acta Crystallogr. A71 (2015) 3-8
10.1107/S2053273314026370

[20] http://www.ccdc.cam.ac.uk/conts/retrieving.html (or from the CCDC, 12 Union Road, Cambridge CB2 1EZ, UK; Fax: +44 1223 336033; E-mail: deposit@ccdc.cam.ac.uk).

[21] DIAMOND - Crystal and Molecular Structure Visualization
K. Brandenburg
Crystal Impact GbR, Bonn, Germany, 2014.

[22] Structure of $BaGd_2(MoO_4)_4$ crystal
Zhao Dan, Lin Zhou Bin, Wang Guo Fu
Chinese J. Struc. Chem. 26 (2007) 328-332.

[23] Comprehensive derivation of bond-valence parameters for ion pairs involving oxygen
O.C. Gagne and F.C. Hawthorne
Acta Crystallogr. B71 (2015), 562-578.
10.1107/S2052520615016297

[24] https://www.iucr.org/resources/data/datasets/bond-valence-parameters

[25] Revised Effective Ionic Radii and Systematic Studies of Interatomic Distances in Halides and Chalcogenides,
R.D. Shannon
Acta Cryst. A 32 (1976) 751-767.
10.1107/S0567739476001551

[26] Barium-lanthanide double molybdates $BaLn_2(MoO_4)_4$. II. Crystal structure of $BaNd_2(MoO_4)_4$
Kiseleva I.I., Sirota M.I., Ozerov R.P., Balakireva T.P., Maier A.A.
(1) Sov. Phys. Crystallogr. 24 (1979) 730-732.
(2) Kristallografiya 24 (1979) 1277-1279.

[27] Infrared and Raman Spectra of Inorganic and Coordination Compounds
K. Nakamoto
Mir, Moscow, Russia, 1966.

[28] Electrical and Vibrational Studies of $Na_2K_2Cu(MoO_4)_3$
Wassim Dridi, Mohamed Faouzi Zid , Miroslaw Maczka
Advances in Materials Science and Engineering 2017 (2017) Article ID 6123628,
10.1155/2017/6123628

[29] Exploration of structural, vibrational and spectroscopic properties of self-activated orthorhombic double molybdate $RbEu(MoO_4)_2$ with isolated MoO_4 units
V. V. Atuchin, A. S. Aleksandrovsky, B. G. Bazarov, J. G. Bazarova, O. D. Chimitova, Y. G. Denisenko, T. A. Gavrilova, A. S. Krylov, E. A. Maximovskiy, M. S. Molokeev, A. S. Oreshonkov,A. M. Pugachev, Ni. V. Surovtsev
J. Alloys Compd. 785, (2019) 692-697.
10.1016/j.jallcom.2019.01.013

[30] Crystal growth, IR specular reflectance and polarized Raman studies of $LiNa_5Mo_9O_{30}$ polar single crystal
M. Ptak, A. Majchrowski, A. Sieradzki, M. Suszyńska, M. Mączka
Spectrochim. Acta A Mol. Biomol. Spectrosc. 228 (2020) 117850
10.1016/j.saa.2019.117850